



## NONCONTACTING PHOTOTHERMAL RADIOMETRY OF SiO<sub>2</sub>/Si MOS CAPACITOR STRUCTURES

A. SALNICK<sup>1</sup>, C. JEAN<sup>2</sup> and A. MANDELIS<sup>1</sup>

<sup>1</sup>Photothermal and Optoelectronic Diagnostics Laboratories, Department of Mechanical Engineering, University of Toronto, 5 King's College Road, Toronto, Ontario M5S 3G8, Canada

<sup>2</sup>MITEL S.C.C., Bromont, Québec J0E 1L0, Canada

(Received 19 March 1996; in revised form 12 June 1996)

**Abstract**—An infrared photothermal radiometric (PTR) method has been applied to the SiO<sub>2</sub>/Si interface noncontact diagnostics. Both photothermal frequency-domain (PTR-FD) and photothermal deep-level transient spectroscopy (PTR-DLTS) analyses have been performed on two full-size Si wafers containing Al and poly-Si gated MOS structures. A new fitting procedure which uses both the PTR-FD amplitude and phase frequency responses is proposed allowing the measurements of the values of the carrier diffusivity, lifetime and surface recombination velocity. A behavior consistent with photoinjected carrier lifetime enhancement due to trap thermal filling at elevated temperatures has been observed on both wafers. The activation energies measured by the two photothermal techniques are found to be close: 0.15–0.17 eV and 0.21 eV below the bottom of the conduction band for Al-gated and poly-Si gated wafers, respectively. © 1997 Elsevier Science Ltd. All rights reserved

### 1. INTRODUCTION

The measurements of photoexcited excess carrier lifetime and activation energies in a semiconductor are useful in the characterization of the quality of semiconductor materials and in evaluating the performance of working semiconductor devices. The noncontact method of photothermal infrared radiometry (PTR), with both frequency-domain (PTR-FD)[1–3] and rate-window (PTR-RW)[4,5] detection configurations has been shown to be promising for remote on-line or off-line impurity/electronic defect diagnostics. A new PTR deep-level transient spectroscopy (PTR-DLTS) which combines the PTR-RW with semiconductor temperature ramping has been developed recently[6] and found to possess high spectral peak separation and spatial resolution.

In the present paper we report the first results of the off-line quality control analysis of SiO<sub>2</sub>/Si interfaces of full-size Si wafers with MOS structures by using the PTR-FD and PTR-DLTS methods. For the PTR-FD technique we propose a new fitting procedure which uses not only the amplitude frequency responses[1–3], but also employs the phase dependencies which are shown to be more sensitive to changes in carrier diffusivity ( $D_n$ ), carrier lifetime ( $\tau$ ) and surface recombination velocity ( $s$ ).

### 2. THEORETICAL MODEL

To derive the PTR signal from a plasma-dominated semiconductor we will consider the wafer of thickness  $L$  with the front surface lying at  $x = 0$  and

highly scattering (unpolished) back surface. With the excitation laser beam off, the total i.r. radiation power  $P_{\text{off}}(\lambda)$  arriving at the front surface (area  $A$ ) of the wafer at ambient temperature  $\Theta_a$  is:

$$P_{\text{off}}(\lambda) = \int_0^L \alpha_{\text{IR}}(x, \lambda) \exp \left[ - \int_0^x \alpha_{\text{IR}}(x', \lambda) dx' \right] dx \quad (1)$$

where  $\alpha_{\text{IR}}$  is the IR absorption coefficient of the semiconductor at the wavelength  $\lambda$ . The total power registered by the IR detector is:

$$Q_{\text{off}} = \int_{\lambda_1}^{\lambda_2} [1 - R(\lambda)] W_s(\lambda, \Theta_a) P_{\text{off}}(\lambda) d\lambda \quad (2)$$

where  $R(\lambda)$  is the IR reflectance of the semiconductor polished surface,  $\lambda_1$  and  $\lambda_2$  are the lower and upper wavelengths of the IR detector response and

$$W_s(\lambda, \Theta_a) = \frac{2\pi hc^2 A}{\lambda^5 [\exp(hc/\lambda k \Theta_a) - 1]} \quad (3)$$

is Planck's distribution function.

For Si  $\alpha_{\text{IR}}(x, \lambda)$  is dominated by weak lattice absorption in the absence of laser irradiation ( $\alpha_{\text{IR,Si}} \cong 1.2 \text{ cm}^{-1}$ , [7]). For  $L \leq 500 \mu\text{m}$ ,  $\alpha_{\text{IR}} L \ll 1$  and the radiation power can be approximated:

$$\begin{aligned} P_{\text{off}}(\lambda) &\approx \int_0^L \alpha_{\text{IR}}(x, \lambda) \left[ 1 - \int_0^x \alpha_{\text{IR}}(x', \lambda) dx' \right] dx \\ &\approx \int_0^L \alpha_{\text{IR}}(x, \lambda) dx. \end{aligned} \quad (4)$$

With the laser beam on,  $\alpha_{IR}(x, \lambda)$  increases due to the presence of photo-injected carriers:

$$\alpha'_{IR}(x, \lambda) = \alpha_{IR}(x, \lambda) + \Delta\alpha_{FC}(x, \lambda). \quad (5)$$

The change in the reflection coefficient  $R(\lambda)$  is assumed negligible, since,[8]:

$$\frac{\Delta R}{R} = -\frac{2e^2\lambda^2}{4\pi n c^2 \epsilon_0 m(n^2 - 1)} \Delta N(0) \quad (6)$$

and at  $\lambda = 10 \mu\text{m}$ , for intrinsic Si with photo-injected carrier density  $\Delta N(0) = 10^{18} \text{ cm}^{-3}$   $\Delta R = -7.7 \times 10^{-21} \Delta N(0) = -7.7 \times 10^{-3}$ . The temperature rise in the semiconductor changes the Planck function, eqn (3),  $\Theta_a \rightarrow \Theta_s = \Theta_a + \Delta\Theta$ , so as

$$\Delta W_s(\lambda, \Theta_a + \Delta\Theta) \cong W_s(\lambda, \Theta_a) + \left( \frac{\partial W_s}{\partial \Theta_a} \Big|_{\Theta = \Theta_a} \right) \Delta\Theta \quad (7)$$

and

$$\Delta\Theta \left( \frac{\partial W_s}{\partial \Theta_a} \right) = \frac{W_s(\lambda, \Theta_a)}{\exp(hc/\lambda k \Theta_a) - 1} \left( \frac{hc}{\lambda k \Theta_a} \right) \frac{\Delta\Theta}{\Theta_a}. \quad (8)$$

When thermal-wave effects are not dominant,  $\Delta\Theta/\Theta_a \ll 1$ , so Planck's function can be assumed

constant in a plasma-dominated wafer. Assuming that the photo-injected carrier density is limited to  $10^{19} \text{ cm}^{-3}$  by lifetime reduction due to Auger recombination[9,10]:

$$[\alpha'_{IR}(x, \lambda)]_{\text{max}} L \ll 1 \Rightarrow \exp \left[ - \int_0^x \alpha'_{IR}(x', \lambda) dx' \right] \cong 1 - \int_0^x \alpha'_{IR}(x', \lambda) dx \quad (9)$$

the radiation power with the laser on can be written:

$$P_{\text{on}}(\lambda) \cong \int_0^L \alpha_{IR}(x, \lambda) dx + \int_0^L \Delta\alpha_{FC}(x, \lambda) dx. \quad (10)$$

The a.c. PTR signal in the i.r. detection is equal to

$$\Delta Q = Q_{\text{on}} - Q_{\text{off}} \quad (11)$$

so that by combining eqns (1)–(2) and (10)

$$\Delta Q = \int_{\lambda_1}^{\lambda_2} [1 - R(\lambda)] W_s(\lambda, \Theta_a) \times d\lambda \int_0^L \Delta\alpha_{FC}(x, \lambda_{\text{vis}}) dx \quad (12)$$

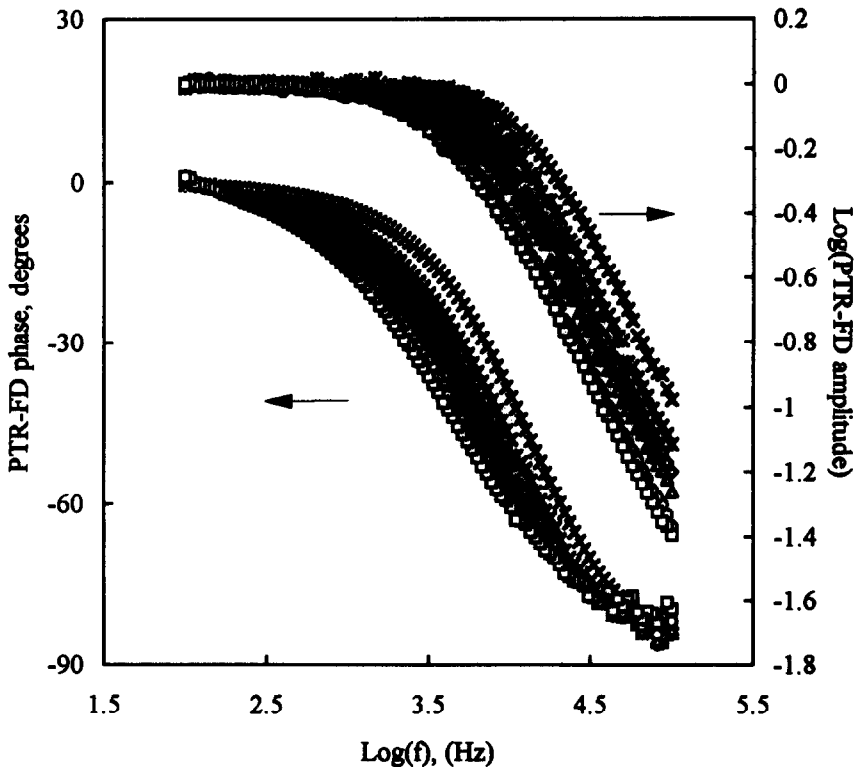


Fig. 1. The PTR-FD amplitude and phase frequency responses of sample W2 measured at different temperatures: 298 K (x), 323 K (\*), 348 K (◇), 373 K (△), 398 K (○) and 423 K (□). The amplitude curves are normalized at low frequencies.

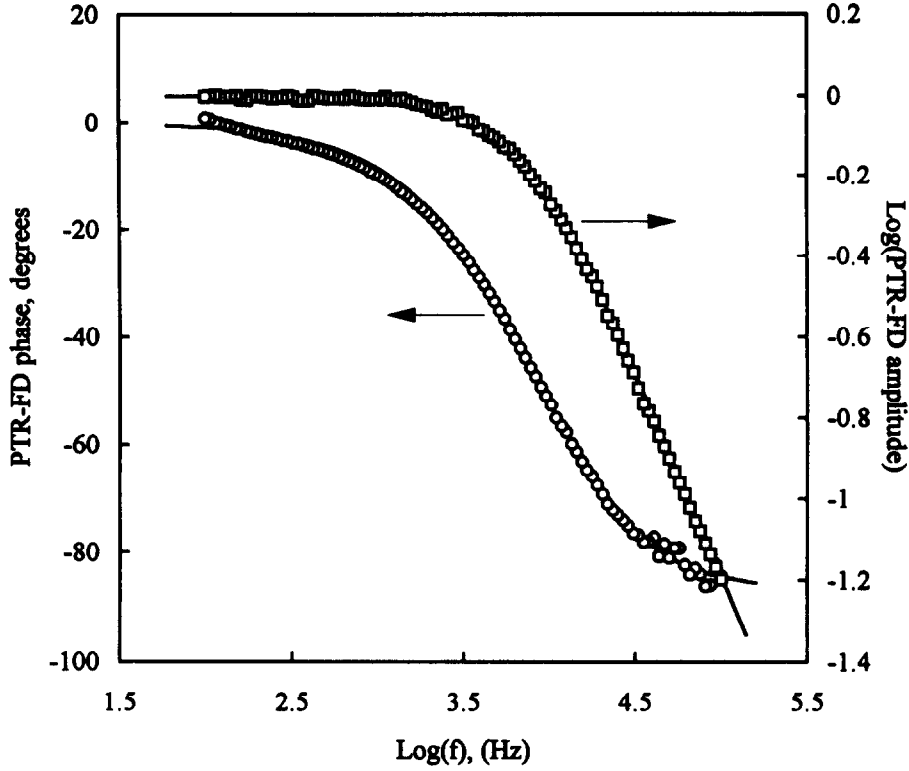


Fig. 2. The PTR-FD amplitude ( $\square$ ) and phase ( $\circ$ ) frequency responses of sample W2 obtained at 348 K and the results of the best fitting (lines) with  $D_n = 10 \text{ cm}^2 \text{ s}^{-1}$ ,  $s = 150 \text{ cm s}^{-1}$  and  $\tau_{\text{FD}} = 36 \mu\text{s}$ .  $\tau_{\text{FD}}$  stands for frequency-domain measurements of the lifetime.

given that the wavelength that matters in the difference  $P_{\text{on}}(\lambda, \lambda_{\text{vis}}) - P_{\text{off}}(\lambda)$  is that of the photoexciting laser,  $\lambda_{\text{vis}}$ . The vis dependence appears in the integral  $\int_0^L \Delta\alpha_{\text{FC}}(x, \lambda_{\text{vis}}, \lambda) dx$ . Letting

$$J_{\text{FC}}(\lambda_{\text{vis}}, \lambda) \equiv \int_0^L \Delta\alpha_{\text{FC}}(x, \lambda_{\text{vis}}, \lambda) dx. \quad (13)$$

equation (12) yields

$$\Delta Q(\lambda_{\text{vis}}) = \int_{\lambda_1}^{\lambda_2} C(\lambda, \Theta_a) J_{\text{FC}}(\lambda_{\text{vis}}, \lambda) d\lambda \quad (14)$$

where

$$C(\lambda, \Theta_a) \equiv [1 - R(\lambda)] W_s(\lambda, \Theta_a). \quad (15)$$

A classical model for the wave propagation in a free carrier plasma gives[11]:

$$\begin{aligned} \Delta\alpha_{\text{FC}}(x, \lambda_{\text{vis}}, \lambda) &= \frac{\lambda^2 e^3}{4\pi c^3 n \epsilon_0 m^2 \mu} \Delta N(x, \lambda_{\text{vis}}) \\ &\equiv \xi(\lambda) \Delta N(x, \lambda_{\text{vis}}) \end{aligned} \quad (16)$$

where  $\mu$  is the mobility which depends on carrier density, especially at high densities. It is assumed independent of  $\Delta N$  here. Finally we obtain:

$$\begin{aligned} \Delta Q(\lambda_{\text{vis}}) &= \int_{\lambda_1}^{\lambda_2} \xi(\lambda) [1 - R(\lambda)] \\ &\quad \times W_s(\lambda, \Theta_a) d\lambda \int_0^L \Delta N(x, \lambda_{\text{vis}}) dx \end{aligned} \quad (17)$$

or

$$\Delta Q(\lambda_{\text{vis}}) = C_2(\lambda_1, \lambda_2) \int_0^L \Delta N(x, \lambda_{\text{vis}}) dx \quad (18)$$

where

$$C_2(\lambda_1, \lambda_2) \equiv \int_{\lambda_1}^{\lambda_2} \xi(\lambda) [1 - R(\lambda)] W_s(\lambda, \Theta_a) d\lambda. \quad (19)$$

Equation (18) indicates that the PTR signal from plasma-dominated semiconductors depends on the number of photo-injected carriers integrated over the thickness of the wafer. This result, eqns (18)–(19), is similar to that obtained earlier semi-empirically[1,3].

Taking the one-dimensional distribution of the photo-injected carrier plasma density in a semicon-

ductor with high optical absorption to be of the form[1,4,12,13]:

$$\Delta N(x) = \frac{N_0}{\sigma_n D_n + s} e^{-\sigma_n x} \quad (20)$$

where  $N_0$  is the number of photo-injected carriers at the surface,  $s$  is the surface recombination velocity and the complex plasma-wave vector  $\sigma_n$  is defined as:

$$\sigma_n = \sqrt{\frac{1 + i\omega\tau}{D_n\tau}}, \quad (21)$$

we obtain upon calculating the integral in eqn (18):

$$\Delta Q = \frac{N_0}{\sigma_n^2 D_n + \sigma_n s} C_2(\lambda_1, \lambda_2) \quad (22)$$

assuming  $|\sigma_n|L \gg 1$ .

### 3. EXPERIMENTAL RESULTS AND DISCUSSION

#### 3.1. Experimental set up and samples

Both the PTR-FD and PTR-DLTS instrumentation set-ups used in the present study were described in detail previously[5,6]. An  $\text{Ar}^+$  laser emitting  $\sim 1$  W at 514 nm was used as an excitation source. The modulated square waveform of the laser-beam intensity was controlled by an acousto-optic modulator. The modulation frequency range used was 100 Hz–125 kHz. The lower limit was

chosen so as to prevent the thermal component from dominating the PTR signal. Temperature ramps were introduced by a heater/temperature controller with the entire process controlled by the computer. Special arrangements of the set up have been made to fit the large-size wafers (diameter 10 cm). The heating system was capable of varying and maintaining the sample temperature up to 473 K.

Two Si wafers from MITEL S.C.C. (Bromont, Quebec, Canada) containing multiple MOS capacitor structures were studied in the present work. An Al-gated MOS structure (sample W1) had the following parameters: Al layer thickness 0.8  $\mu\text{m}$ , oxide thickness 0.1  $\mu\text{m}$ ,  $n$ -Si substrate with resistivity  $\rho = 10\text{--}15\Omega\text{cm}$  and impurity level of  $N \sim 2.5 \times 10^{14} \text{cm}^{-3}$ . The gate area was  $2.1 \times 10^{-2} \text{cm}^2$ .

In sample W2 the gate was  $n$ -type poly-Si of 0.35  $\mu\text{m}$  thickness and  $\rho = 30\Omega\text{cm}$  with  $2.35 \times 10^{-3} \text{cm}^2$  gate area. The oxide thickness was 0.08  $\mu\text{m}$  and the substrate was  $n$ -Si with  $\rho = 10\text{--}15\Omega\text{cm}$  and  $N \sim 9 \times 10^{14} \text{cm}^{-3}$ .

#### 3.2. PTR-FD measurements

The PTR-FD frequency scans on sample W2 were obtained by direct illumination of one of the poly-Si gate islands. In this case the optical absorption length at 514 nm excitation wavelength is longer than both gate and oxide thickness ( $1/\lambda_{\text{Si}} \approx 1 \mu\text{m}$ ) thus allowing

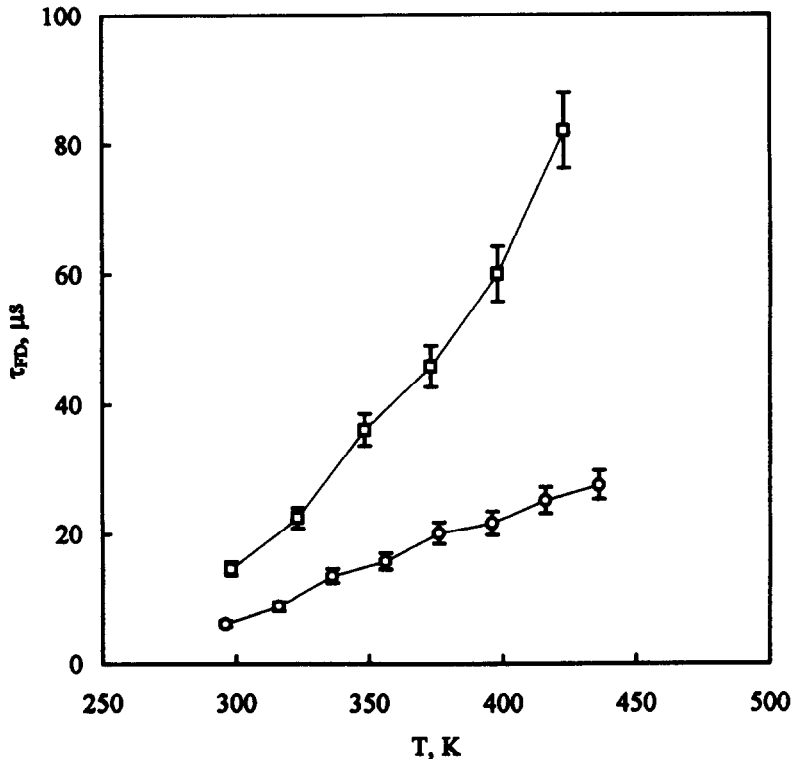


Fig. 3. PTR-FD lifetime temperature dependencies of sample W1 (O) and W2 (□) obtained by fitting the PTR-FD amplitude and phase frequency responses of Fig. 1.

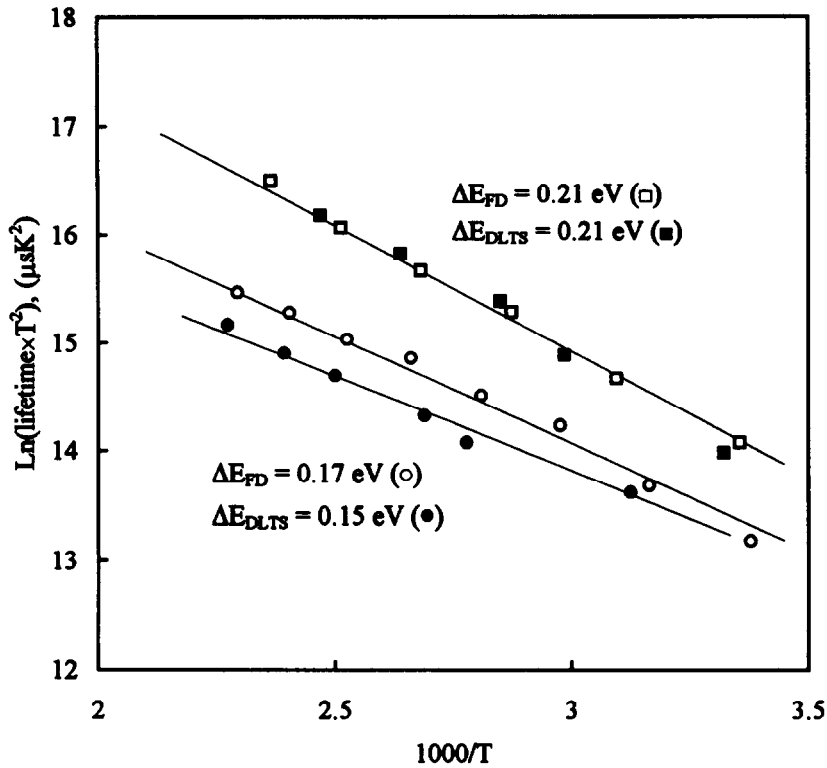


Fig. 4. Arrhenius plots of the PTR-FD and PTR-DLTS lifetimes of samples W1 (circles) and W2 (rectangles) and corresponding energy levels.

a significant number of photo-injected carriers to be created at the SiO<sub>2</sub>/Si interface. Here the PTR-FD signal is dominated by plasma effects. However, for sample W1, which had a thick and highly reflective Al-gate layer, initial PTR-FD frequency scans performed through the gate showed a strong influence of the thermal waves. Therefore, all the measurements on that sample were performed on the oxide side where the PTR-FD signal frequency behavior was found to be similar to that of sample W2, i.e. purely electronic.

The PTR-FD amplitude and phase frequency responses of sample W2 at different temperatures are presented in Fig. 1. The PTR-FD amplitude increases with increasing temperature due to the Stefan-Boltzmann law-based nature of the PTR-signal and increasing number of thermally injected carriers (in Fig. 1 the amplitude curves are normalized to outline only the changes in shape with temperature). The frequency behavior of the PTR-FD amplitude and phase frequency responses can be clarified by the following simple analysis. Taking the logarithm of the PTR-FD signal calculated in the previous section, eqn (22), we obtain:

$$\text{Log}_{10}(\Delta Q) = \text{const} - \text{Log}_{10} \left( \frac{1 + i\omega\tau}{\tau} + s \sqrt{\frac{1 + i\omega\tau}{D_n\tau}} \right) \quad (23)$$

where const is a normalization parameter. Correspondingly, at low modulation frequencies when  $\omega\tau \ll 1$ :

$$\text{Log}_{10}(\Delta Q) = \text{const} - \text{Log}_{10} \left( \frac{1}{\tau} + sL_n^{-1} \right) \quad (24)$$

where  $L_n \equiv \sqrt{D_n\tau}$  is the photo-injected carrier diffusion length. So, both the PTR-FD amplitude (which is essentially  $|\Delta Q|$ ) and phase ( $\tan^{-1}(\text{Im}(\Delta Q)/\text{Re}(\Delta Q))$ ) are frequency-independent with the phase saturated at zero value. At the high frequency limit,  $\omega\tau \gg 1$ , eqn (23) is simplified to

$$\text{Log}_{10}(\Delta Q) = \text{const} - \text{Log}_{10} \left( i\omega + s \sqrt{\frac{i\omega}{D_n}} \right) \quad (25)$$

and in a Log-Log plot the PTR-FD amplitude decreases with the constant slope of  $-1$  in the case of low recombination velocities and between  $-1$  and  $-0.5$  for higher  $s$ . Here the PTR-FD signal is independent of  $\tau$ . Thus, the values of  $\tau$ ,  $D_n$  and  $s$  can be evaluated by a multiparameter fitting of the experimental data to the theoretical model, eqn (23).

Both the PTR-FD amplitude and phase frequency responses shown in Fig. 1 perfectly follow the predictions of the theory. The constant high-frequency slope of  $-1$  observed for all amplitude curves indicates a very low surface recombination of SiO<sub>2</sub>/Si

interface which practically does not change with temperature (the values of  $s$  obtained by three-parameter fitting were in the range of  $100\text{--}300\text{ cm s}^{-1}$ ). However, the carrier lifetime shows a clear increasing tendency as the slope intersection frequency position in the amplitude curves of Fig. 1 moves towards lower frequency with increasing temperature.

Figure 2 represents typical results of the three-parameter fitting of the PTR-FD amplitude and phase frequency responses by the theoretical model. The correlation is very good both for amplitude and phase. It should be noted that the phase dependencies ignored in the previous studies[1,3] are of significant importance for the fitting procedure as they allow, under low  $s$  conditions a two-parameter fitting ( $\tau$ ,  $D_n$ ) using two sets of independent data, thus decreasing the computational uncertainties. Besides, the PTR-FD phase dependencies being independent of the surface reflectance, are found to be more sensitive to changes in  $\tau$  and  $D_n$  at low frequencies than the amplitude responses which makes them very useful, especially in temperature studies when all the adjustable parameters are temperature dependent.

A similar analysis was applied to the PTR-FD data obtained from sample W1. The lifetime temperature dependencies are plotted in Fig. 3, along with those of sample W2. The increase in  $\tau$  with temperature observed for both wafers follows the Shockley-Read-

Hall theory[14-16] which assumes that the thermally increased density of intrinsic carriers fills up existing trapping sites and thus increases the photo-injected carrier lifetime. For the carrier diffusivity we found a decreasing temperature dependence for both samples proportional to  $\sim T^{-1.5}$  which is in reasonable agreement with known[17] and photothermally measured[18,19] rates. The corresponding Arrhenius plots of the PTR-FD lifetimes and the calculated activation energies are presented in Fig. 4 along with the PTR-DLTS data of the next section. The energy value of  $\Delta E = 0.21\text{ eV}$  obtained for sample W2 is probably due to the near-interface shallow electron trap produced during the gate layer growth.

The fact that the poly-Si-gated MOS have a very low level of damage at the  $\text{SiO}_2/\text{Si}$  interface was confirmed by C-V measurements, exhibiting the surface state density of  $6 \times 10^{10}\text{ cm}^{-2}$  while the same value for the Al-gated MOS was found to be  $4 \times 10^{11}\text{ cm}^{-2}$ . This difference results in lower  $\tau_{\text{FD}}$  of W1 sample with respect to that of W2.

### 3.3. PTR-DLTS measurements

The PTR-DLTS signal from semiconductors due to photo-injected carriers originates from the contribution of each free carrier to the black-body emission measured by the i.r. detector, so that the theoretical model of Section 2 is also applicable in

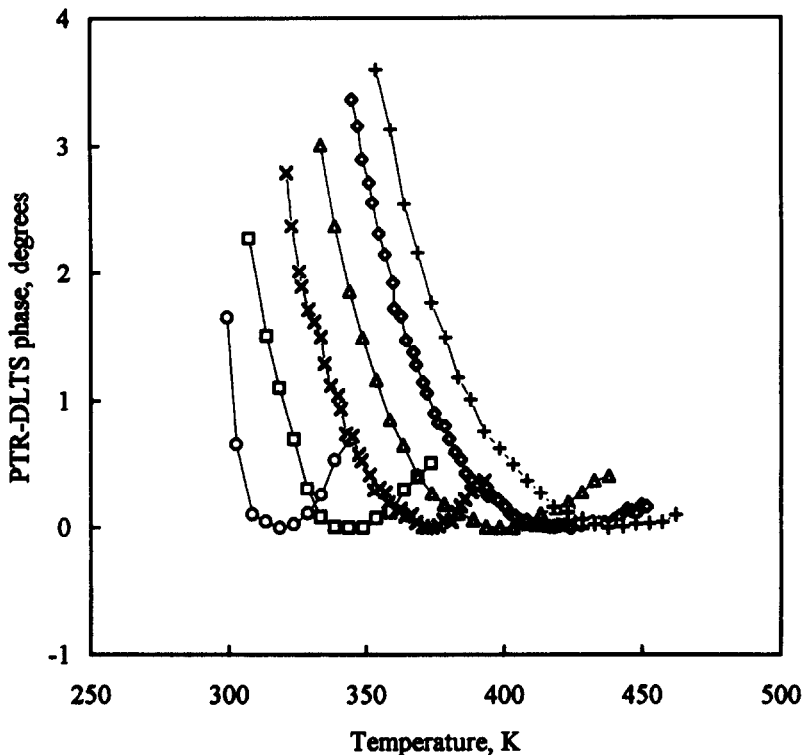


Fig. 5. Normalized PTR-DLTS phase spectra of sample W2 with different pulse repetition periods ( $T_0$ ):  $8\text{ }\mu\text{s}$  ( $\circ$ ),  $10\text{ }\mu\text{s}$  ( $\square$ ),  $12\text{ }\mu\text{s}$  ( $\times$ ),  $15\text{ }\mu\text{s}$  ( $\triangle$ ),  $17\text{ }\mu\text{s}$  ( $\diamond$ ) and  $20\text{ }\mu\text{s}$  ( $+$ ). Duty cycle  $\tau_p/T_0 = 50\%$ . Only the part of each spectrum close to the minimum is shown.

this case. In the present study we used the lock-in PTR-DLTS detection which has higher signal-to-noise ratio than gated boxcar integration [20].

The PTR-DLTS temperature scans of both wafers were performed with fixed ratio of the pulse duration ( $\tau_p$ ) to the pulse repetition period ( $T_0$ ) (duty cycle) equal to 50%. Both the PTR-DLTS magnitude and phase were recorded as a function of sample temperature at different  $T_0$ . Figure 5 represents some typical PTR-DLTS phase spectra obtained on Sample W1. As in the case of the PTR-FD studies the phase temperature dependencies were found to be important here and more sensitive to the presence of the DLTS-peaks than those of the in-phase or quadrature component of the PTR-DLTS signal. Neither the in-phase, nor the quadrature temperature dependencies corresponding to the phase data shown in Fig. 5 exhibited any extrema in the temperature/repetition period range used. Because of the fact that the phase changes near the peak (minimum) value were on the order of several degrees, their reproducibility was very good.

The PTR-DLTS lifetime which was assumed to be proportional to  $T_0(\tau(T_m) = \eta T_0)$  where  $T_m$  is the PTR-DLTS peak temperature, was found to increase with increasing temperature for both samples as  $T_m$  shifted to higher temperatures with increasing  $T_0$  (Fig. 5), behavior consistent with that found by the PTR-FD method. The Arrhenius plots of the PTR-DLTS lifetimes and the calculated activation energies are presented in Fig. 4. The same value of 0.21 eV was found for the poly-Si gated sample W2 while the W1 sample exhibits the energy level of 0.15 eV, i.e. slightly lower than that of PTR-FD method (0.17 eV). In principle, the correlation between both methods in energy levels is good for both sample W1 and W2.

Finally, the PTR-FD ( $\tau_{FD}$ ) and PTR-DLTS ( $T_0$ ) lifetimes were compared assuming a linear relation between them. The results are summarized in Table 1 where the PTR-FD lifetimes were taken at the corresponding peak temperatures ( $T_m$ ) of the PTR-DLTS spectra. As can be seen from this table, the foregoing lifetimes are related to each other through the constant  $\eta \approx 1.3$ , which is nearly the same for both samples and for all values of  $T_0$  used,

Table 1. Relation between the PTR-DLTS ( $T_0$ ) and PTR-FD ( $\tau_{FD}$ ) lifetimes

Sample	$T_0, \mu\text{s}$	$T_m, \text{K}$	$\tau_{FD}, \mu\text{s}$	$\eta = \frac{\tau_{FD}(T_m)}{T_0}$
W1	8	320	10	1.31
W1	10	360	13	1.30
W1	12	372	16	1.33
W1	15	400	20	1.33
W1	17	418	24	1.41
W1	20	437	27	1.35
W2	10	298	14	1.40
W2	20	335	26	1.30
W2	30	351	40	1.33
W2	40	380	52	1.30
W2	50	405	65	1.30

thus validating the proportionality assumption between  $T_0$  and  $\tau(T_m)$ .

#### 4. SUMMARY

In the present work the SiO<sub>2</sub>/Si interfaces of two different MOS capacitor structures, Al-gated (wafer W1) and poly-Si-gated (wafer W2), were studied by using noncontacting photothermal methods. The results of the quantitative analysis of the interfaces in terms of carrier transport parameters and activation energies by photothermal frequency-domain and DLTS methods were in good agreement and showed an increased carrier lifetime at elevated temperatures. Shallow electron traps at  $\sim 0.16$  and 0.21 eV were found for samples W1 and W2, respectively, by using both techniques, and are assumed to be produced during the gate layer growth.

*Acknowledgements*—We wish to gratefully acknowledge the support of the Natural Sciences and Research Council of Canada (NSERC) for a Collaborative Research Grant. One of us (A.S.) is also grateful to NSERC for a NATO Science Research Fellowship Award.

#### REFERENCES

1. S. J. Sheard, M. G. Somekh and T. Hiller, *Mater. Sci. Engng* **B5**, 101 (1990).
2. T. M. Hiller, M. G. Somekh, S. J. Sheard and D. R. Newcombe, *Mater. Sci. Engng* **B5**, 107 (1990).
3. S. Sheard and M. Somekh, *Progress in Photoacoustic and Photoacoustic Science and Technology, Vol. II: Nondestructive Evaluation (NDE)* (Edited by A. Mandelis), pp. 112–150. Prentice Hall, Englewood Cliffs, NJ (1994).
4. A. Mandelis and Z. H. Chen, *Rev. Sci. Instrum.* **63**, 2977 (1992).
5. Z. H. Chen, R. Bleiss, A. Mandelis, A. Buczkowski and F. Shimura, *J. Appl. Phys.* **73**, 5043 (1993).
6. A. Mandelis, R. A. Budiman, V. Vargas and D. Wolff, *Appl. Phys. Lett.* **67**, 1582 (1995).
7. I. W. Boyd, T. D. Binnie, J. I. B. Wilson and M. J. Coles, *J. Appl. Phys.* **55**, 3061 (1984).
8. A. Rosencwaig, *Photoacoustic and Thermal-Wave Phenomena in Semiconductors*, (Edited by A. Mandelis), p. 103. Elsevier, New York (1987).
9. L. Passari and E. Susi, *J. Appl. Phys.* **54**, 3935 (1983).
10. E. J. Yoffa, *Phys. Rev. B* **21**, 2415 (1980).
11. S. Ramo, J. R. Whinnery and T. Van Duzer, *Fields and Waves in Communication Electronics*, p. 334. Wiley, New-York (1965).
12. A. C. Boccara and D. Fournier, *Photoacoustic and Thermal-Wave Phenomena in Semiconductors* (Edited by A. Mandelis), p. 291. Elsevier, New York (1987).
13. N. Mikoshiba, H. Nakamura and K. Tsubouchi, In: *Proc. IEEE Ultrasonic Symp.*, p. 580 (1982).
14. R. N. Hall, *Phys. Rev.* **87**, 387 (1952).
15. W. Shockley and W. T. Read, *Phys. Rev.* **87**, 835 (1952).
16. A. Oshawa, K. Honda, R. Takizawa and M. Toyokura, *Rev. Sci. Instrum.* **54**, 210 (1983).
17. S. M. Sze, *Physics of Semiconductor Devices*, 2nd edn, p. 29. Wiley, New York (1981).
18. K. V. Lapshin, A. N. Petrovsky and A. Salnick, *Tech. Phys. Lett.* **19**, 9 (1993).
19. K. V. Lapshin, A. N. Petrovsky, A. Salnick and V. V. Zuev, *Tech. Phys. Lett.* **20**, 880 (1994).
20. Z. H. Chen and A. Mandelis, *Phys. Rev. B* **46**, 13256 (1992).